UCID- 20933

FEM3 DISPERSION CALCULATIONS EVALUATION OF TURBULENCE SUBMODEL

Donald L. Ermak
Stevens T. Chan

October 1986

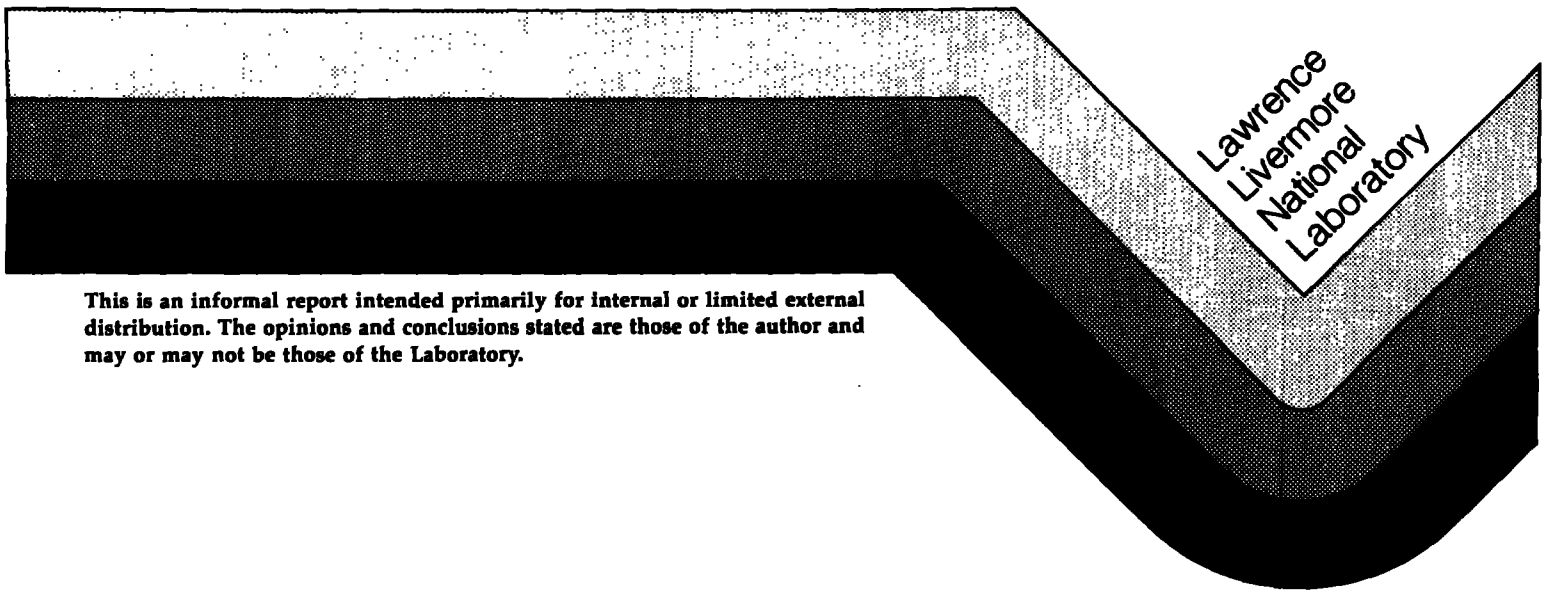

Printed in the United States of America
Available from
National Technical Information Service
U.S. Department of Commerce
5285 Port Royal Road
Springfield, VA 22161

Price Code	Page Range
A01	Microfiche
Papercopy Prices	
A02	001-050
A03	051-100
A04	101-200
A05	201-300
A06	301-400
A07	401-500
A08	501-600
A09	601

FEM3 DISPERSION CALCULATIONS: EVALUATION OF TURBULENCE SUBMODEL

1. INTRODUCTION

FEM3 is a three-dimensional computer model that was designed to simulate the atmospheric dispersion of large heavier-than-air gas releases (Chan, 1983). The model employs a modified finite element method (Gresho et al., 1984) to solve the time-dependent conservation equations of mass, momentum, energy, and species along with the ideal gas law for the equation of state. Turbulence is treated by using a K-theory submodel. These equations provide a mathematical description of the physics of heavy gas dispersion including gravity spread, the effect of density stratification on turbulent mixing, and ground heating into the cloud and its effects on density stratification and turbulence. In addition, FEM3 can treat flow over variable terrain and around obstructions such as cylinders and cubes. Since it is fully three-dimensional, FEM3 can simulate complicated cloud structures such as the vortices that are typical of dense gas flows, cloud bifurcation that has been observed during heavy gas releases under low windspeed, stable, ambient conditions, and cloud deflection caused by sloping terrain.

The development of FEM3 has been part of a larger research effort over the past eight years by the Lawrence Livermore National Laboratory (LLNL) to study the atmospheric dispersion of denser-than-air releases. This research has been conducted under several sponsors and has centered about a sequence of field scale test series involving a variety of release gases. LLNL performed liquefied natural gas (LNG) field tests for the U.S. Department of Energy (DOE) in 1978 and 1980 (Koopman et al., 1982), and again in 1981 with additional sponsorship by the Gas Research Institute (Goldwire et al., 1983). In 1983 LLNL performed ammonia dispersion tests for the U.S. Coast Guard and The Fertilizer Institute (Goldwire et al., 1985) and nitrogen

tetroxide spill experiments for the U.S. Air Force (McRae, 1985). Currently, LLNL is conducting hydrogen floride dispersion tests for Amoco Oil Co.

One of the main goals of these test series is to gather data to develop and validate dense gas dispersion models. Over the past few years, the results from FEM3 simulations have been compared with the data obtained from these tests and from a variety of field scale experiments performed by other research groups. These include the LLNL Burro and Coyote series of LNG vapor dispersion experiments (Koopman et al., 1982; Goldwire et al., 1983), the LLNL nitrogen tetroxide [N_2O_4] spill tests (McRae, 1985), and the refrigerated liquid propane spill tests conducted by SHELL Research Limited at Maplin Sands, England (Puttock et al., 1982; Colenbrander et al., 1984).

An early version of FEM3, applied to simulate several of the Burro series experiments, yielded results that correlated quite well with the field data (Ermak et al., 1982). In particular, the model successfully predicted the bifurcated structure of the vapor cloud in the Burro 8 test, which was conducted under low wind speed and stable atmospheric conditions. Since then, FEM3 has been extended to treat variable terrain and the K-theory turbulence submodel has been improved to account for density stratification and ground heat transfer effects. The effect of terrain on the vapor dispersion in specific LNG spills was investigated in Chan et al. (1984). This study demonstrated that, under low wind speed and stable atmospheric conditions, even a relatively gentle terrain can greatly alter the cloud structure and the size and shape of the hazardous area of a heavy gas vapor cloud. Thus, for accurate predictions of heavy gas dispersion in the atmosphere, especially for cases involving gravity-flow dominated regimes, proper treatment of the variable terrain is necessary. The study also provided explanations on the formation of a bifurcated vapor cloud (in the form of horizontal cloud splitting and the vertically, nose-shaped cloud near the edges), due to the action of various outward moving vortices induced by the density gradient in the horizontal directions. A detailed assessment of the FEM3 model using both the Burro and the Coyote series of data can be found in Morgan et al. (1984). In general, the model predictions were observed to correlate quite well with field measurements regarding the maximum downwind distance to the

LFL, cloud shape and size, cloud bifurcation, and the time histories of concentration and temperature at selected locations within the vapor cloud.

To better understand the basic physics involved in the atmospheric dispersion of heavier-than-air gases, a study was conducted primarily to address the heavy gas effects (Ermak and Chan, 1985). Several heavy gas dispersion field experiments were simulated as either a heavier-than-air gas or a neutrally buoyant gas, using the FEM3 model. This study demonstrated that the presence of a heavier-than-air gas has two major effects: (a) reduction of turbulent mixing within the vapor cloud due to the stable stratification of the cloud layer, and (b) generation of gravity spreading and self-induced vortices due to the presence of density gradient in the horizontal directions. These effects are competing in that the former tends to increase concentration levels by decreasing turbulent diffusion and the latter tends to decrease it by entraining air through the top surface and the edges of the vapor cloud. The outcome of the combined effects depends mainly on the atmospheric and spill conditions. Specifically, for spills conducted under unstable atmospheric conditions and low spill rate, the reduction of turbulent mixing appears to be more important, resulting in slightly higher concentrations. On the other hand, for spills conducted under stable atmospheric conditions and high spill rate, the gravity spreading effects are usually more important, resulting in lower concentrations and a shorter downwind distance to the LFL.

More recently, FEM3 was applied to simulate four of the refrigerated liquid propane spill tests conducted by SHELL Research Limited (Chan and Ermak, 1985) The selected propane experiments offer a more direct study of dense-gas effects and represent a severe test of the turbulence submodel used in FEM3 because complicating effects such as those due to aerosols or ground heating are either much less significant or not present. In general, good agreement between model predictions and field data was observed. However, in the case of Spill 54, where an extremely low vapor cloud was produced and heavy gas effects were more profound, the existing turbulence submodel was observed to perform less satisfactorily, thus prompting the development of an improved turbulence submodel discussed in this report.

Other capabilities and applications of the FEM3 model include a submodel for treating aerosol effects in the pressurized ammonia (NH_3) spills (Kansa et al., 1983), the use of FEM3 as a tool for emergency-response planning (Gudiksen et al., 1986), and the development of a phase-change submodel to treat humidity in the ambient atmosphere (Leone et al., 1985).

2. FEM3 TURBULENCE MODEL DEVELOPMENTS

2.1 Model Equations

A detailed description of the FEM3 model is given in Chan (1983) and the numerical method of solution is described in Gresho et al. (1984). The FEM3 model solves the following three-dimensional, time-dependent conservation equations:

$$\frac{\partial(\rho \underline{u})}{\partial t} + \rho \underline{u} \cdot \nabla \underline{u} = -\nabla p + \nabla \cdot (\rho \underline{\underline{K}}^m \cdot \nabla \underline{u}) + (\rho - \rho_h)\, \underline{g} \quad , \tag{2.1.1}$$

$$\nabla \cdot (\rho \underline{u}) = 0, \tag{2.1.2}$$

$$\frac{\partial \theta}{\partial t} + u \cdot \nabla \theta = \frac{1}{\rho C_p} \nabla \cdot (\rho C_p \, \underline{\underline{K}}^{\theta} \cdot \nabla \theta) + \frac{C_{PN} - C_{PA}}{C_p} (\underline{\underline{K}}^{\omega} \cdot \nabla \omega) \cdot \nabla \theta, \tag{2.1.3}$$

$$\frac{\partial \omega}{\partial t} + \underline{u} \cdot \nabla \omega = \frac{1}{\rho} \nabla \cdot (\rho \underline{\underline{K}}^{\omega} \cdot \nabla \omega) \quad , \tag{2.1.4}$$

and

$$\rho = \frac{PM}{RT} = \frac{P}{RT\,(\frac{\omega}{M_N} + \frac{1 - \omega}{M_A})} \quad , \tag{2.1.5}$$

where $\underline{u} = (u, v, w)$ is the velocity, ρ is the density of the mixture, p is the pressure deviation from an adiabatic atmosphere at rest with corresponding density ρ_h, $\underline{g}$ is the acceleration due to gravity, θ is the potential temperature deviation from an adiabatic atmosphere at θ_o, ω is the mass fraction of the dispersed species, $\underline{\underline{K}}^m$, $\underline{\underline{K}}^{\theta}$ and $\underline{\underline{K}}^{\omega}$ are the eddy diffusion tensors for momentum, energy, and the dispersed species, and C_{PN}, C_{PA}, and C_p

are the specific heats for the species, air, and the mixture, respectively. In the equation of state, P is the absolute pressure, R is the universal gas constant, M_N, M_A are the molecular weights of the species and air, and T is the absolute temperature ($T/(\theta + \theta_0) = (P/P_0)^{R/MC_P}$). For problems of current interest, because the heights of interest are generally small (<< 1 km), the ratio P/P_0 is approximately equal to unity and hence no distinction is made between the absolute and potential temperature in the present report. The above set of equations, together with appropriate initial and boundary conditions, are solved by a modified finite element method (Gresho et al., 1984) to yield the ensemble mean values of velocity, pressure, temperature, mass fraction of the dispersed species, and density of the mixture as functions of time and space.

FEM3 treats turbulence by using a K-theory local equilibrium model. The turbulent diffusion tensors $\underline{\underline{K}}^m$, $\underline{\underline{K}}^\theta$, and $\underline{\underline{K}}^\omega$ are assumed to be diagonal and it is further assumed that $\underline{\underline{K}}^\theta = \underline{\underline{K}}^\omega$. Specifically, the vertical diffusion coefficient is given by:

$$K_v = \frac{k[(u_* z)^2 + (w_* h)^2]^{1/2}}{\Phi} \qquad (2.1.6)$$

where

- k = von Karman's constant = 0.4
- u_* = friction velocity = $u_{a*} \cdot |u/u_a|$ in which u is the wind speed and subscript "a" designates the ambient atmosphere
- z = height above ground surface
- w_* = in-cloud "convection velocity" = $\alpha_1[(g/T)\, v_E\, (T_{gr} - T)\, h]^{1/3}$
- α_1 = empirical constant for in-cloud convection = 0.5
- h = cloud height function = $\bar{z} \cdot \exp(1 - z/\bar{z})$
- $\bar{z}$ = characteristic cloud height = $\int \omega \cdot z\, dz / \int \omega\, dz$
- g = acceleration of gravity
- T = cloud temperature
- T_{gr} = ambient ground temperature
- v_E = effective heat-transfer velocity from the ground into the vapor cloud,

The form of the Monin-Obukhov profile function Φ under stable conditions is taken from Dyer (1974) and is defined as

$$\Phi = 1 + 5\ Ri, \qquad Ri \geq 0 \qquad (2.1.7)$$

for all three (momentum, energy, and species) vertical diffusion coefficients. The local Richardson number is, in turn, defined as:

$$Ri = u_*^2 \frac{Ri_a}{(u_*^2 + w_*^2)} + 0.05 \frac{(\rho - \rho_a)}{\rho} \cdot \frac{gh}{(u_*^2 + w_*^2)} \qquad (2.1.8)$$

Herein the first term is designed to include the turbulence in the ambient atmosphere and the second term represents the effects of density stratification, generally a reduction of turbulence in the stably stratified, dense vapor cloud. As can be seen, for isothermal, neutrally buoyant gas or in the absence of a dispersing cloud, the present submodel recovers the ambient diffusivities.

Under neutral ambient conditions ($Ri_a = 0$) with no ground heating ($w_* = 0$), the Richardson number as defined above becomes

$$Ri = \alpha \frac{g(\rho - \rho_a)h}{\rho u_*^2} \qquad (2.1.9)$$

where

$$\alpha = 0.05$$

$$u_* = |u/u_a| \cdot u_{a*}$$

$$h = \bar{z} \cdot \exp(1 - z/\bar{z}) \quad .$$

This model of the Richardson number, Eq. (2.1.9) with the listed definitions of α, u_* and h, will be referred to as Model A.

2.2 Improved Turbulence Submodel

An investigation of the variation of Richardson number with height assuming typical vertical density profiles showed two major deficiencies in the above model:

1) The evaluation of the friction velocity u_* using a scaling factor of the ratio of the resulting flow speed and the ambient wind speed is inappropriate in the source region. Here, the flow velocities are usually very low so that u_* approaches zero and unreasonably large values of the Richardson number are generated.

2) The vertical profile of the Richardson number has a maximum value on the ground surface and monotonically decreases to the ambient value (zero for neutral ambient conditions). Such a shape is inconsistent with intuition which suggests a zero value at ground level and a maximum value near the top of the cloud where the density gradient is largest.

As remedies to what we perceived as deficiencies in the above definition of Richardson number, we looked at two alternative models for Ri using the same form given in Eq. (2.1.9) with different definitions for α, u_*, and h. The first alternative, Model B, uses

$$\alpha = .025$$
$$u_* = u_{a*} \qquad (2.2.1)$$

and

$$h = h_c = \frac{1}{\omega_{max}} \cdot \int \omega dz \quad .$$

The main change in this model is to use a constant friction velocity equal to the ambient value. This change will significantly reduce the large Richardson

numbers that had been calculated in the source region. Also, the value of α has been reduced by a factor of two in accordance with the best fit value obtained in a previous comparison with laboratory experiments (Ermak and Chan, 1986) and the definition of h has been changed slightly for convenience.

The third model, Model C, uses the following parameters,

$$\alpha = \alpha_2 \, nk^2 \, (z/h_c)^n$$

$$u_* = u_{a*} \qquad (2.2.2)$$

$$h = z$$

and

$$h_c = \frac{1}{\omega_{max}} \cdot \int \omega dz$$

This formula for Richardson number was derived by using the following assumptions:

$$Ri = -\alpha_2 \frac{g}{\rho} \frac{(\partial\rho/\partial z)}{(\partial u/\partial z)^2}$$

$$\rho - \rho_a = (\rho - \rho_a)_{z=0} \cdot \exp\,[-(z/h_c)^n] \qquad (2.2.3)$$

and

$$u = \frac{u_*}{k} \ln(z/z_0)$$

In the calculations to be presented here, the exponent n is taken to be 2.0 and the empirical constant $\alpha_2 = 0.2$.

Typical Richardson number profiles (for the source region) obtained with the above models are shown in Fig. 1. As noted above, Model B overcomes the large Richardson number problem in the source region and has larger values

near the top of the cloud. However, the shape of Ri versus height is still similar to Model A. Model C is based upon a more fundamental definition of Richardson number and is seen to address both deficiencies observed in Model A. Therefore, Model C might be expected to out-perform the other two models. To test this hypothesis, we used each of the models to simulate two heavier-than-air wind tunnel tests and compared the calculated results with experimental data.

2.3 Comparison with Wind Tunnel Test Results

Herein we compare the model predictions to test No. 2 and test No. 3 of a three-test series conducted by McQuaid (1976). These experiments were conducted to investigate the structure of shear flows with stable density stratification. The experiments were conducted in a wind tunnel with a fully developed rectangular channel flow of air into which carbon dixoide was introduced through a 'line' source at ground level. Table I lists the main test conditions. Noting the respective source Richardson numbers, dense gas effects would be expected to play a more significant role in test No. 3.

Table I. Test Conditions

	Test 2	Test 3
Source Rate (kg/s)	.0142	.0227
Average Flow Velocity (m/s)	1.83	1.28
Friction Velocity (m/s)	0.0732	0.0528
Source Richardson Number ($Ri = g\,(\rho_s - \rho_a)q_s/\rho_a UU_*^2$)	4.0	17.8

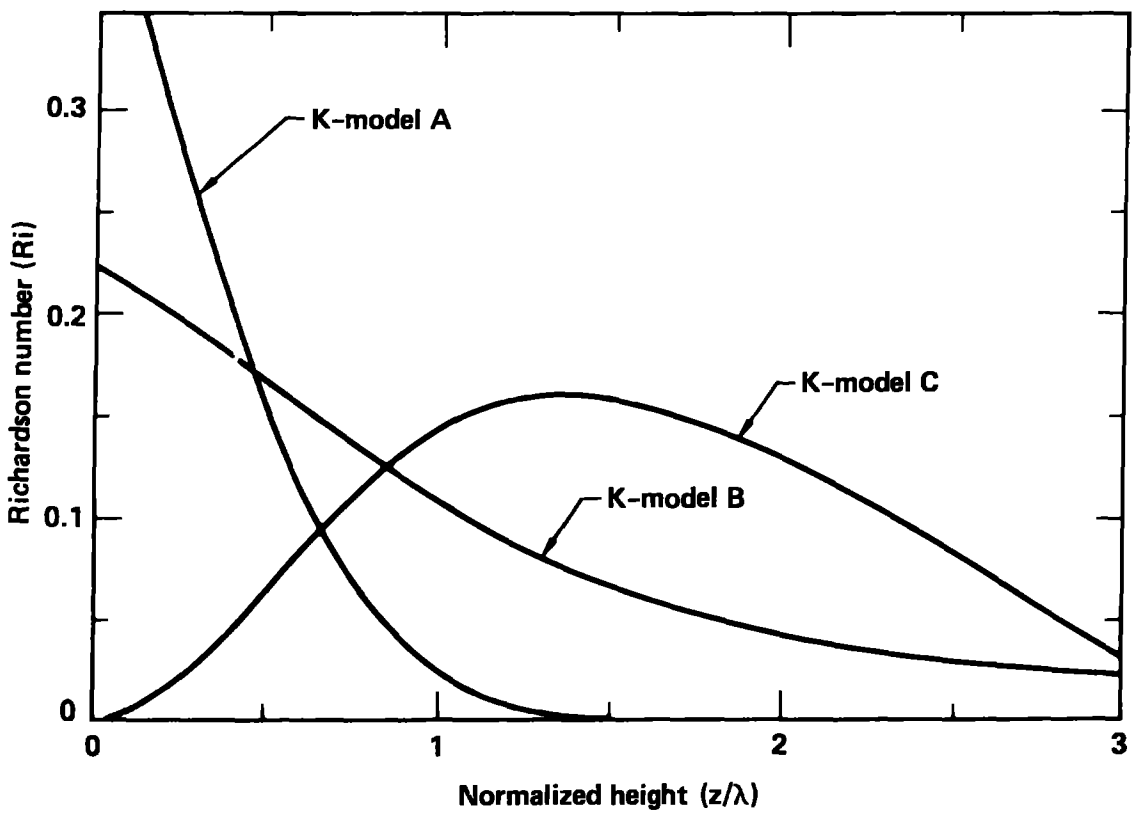

Fig. 1. Typical Richardson number profiles obtained from three different K-theory models (λ being the height with 50% ground level concentration).

Both simulations were conducted using a slightly graded mesh. For Experiment No. 2, the computational domain is x = -0.825 m to 6.0 m, y = 0 to 0.5 m with the source placed at the origin of the coordinate system. A total

number of 3000 mesh points (40 points vertically and 75 points horizontally) were used in the simulation. The inlet velocity profile was based on wind tunnel measurements and specified to be

$$u = \begin{cases} 357.2\ y & \text{m/s} \quad , y \leq 0.00205 \text{ m} \\ 0.174\ \ln(4880\ y) + 0.403 & \text{m/s} \quad , y > 0.00205 \text{ m} \end{cases}$$

The steady state solution was obtained in approximately 6000 steps with a time step size of 0.0025 sec. For Experiment No. 3, the computational domain is $x = -0.82$ m to 6.0 m, $y = 0$ to 0.5 m. A total number of 5000 (50 x 100) mesh points were used. At the inlet, a logarithmic-linear velocity profile in the following form was used

$$u = 0.150857\ [\ln(100{,}000y) + 5y] \quad \text{m/s} \quad .$$

The steady state solution was obtained in approximately 10,000 steps, with a step size of 0.0025 sec. A sample of the predicted results for Experiment No. 3 are shown and compared in Figs. 2 through 7. Fig. 2 shows contour plots of the predicted Richardson number using each of the three models. The maximum Richardson number obtained with model A is seen to be orders of magnitude larger than the maximum value obtained with the other two models. These unrealistically large values occur in the region directly behind (downwind) the source from 0 - 2 m and are due to the very low values of the friction velocity. In Model A, the friction velocity is proportional to the local velocity which approaches zero in the region behind the source. Since the Richardson number is inversely proportional to the square of the friction velocity, it becomes very large as the friction velocity approaches zero. Both Models B and C produce Richardson numbers that are similar in magnitude; however, as expected, the vertical profiles are seen to be quite different. The vertical profile from Model B has a maximum at $z = 0$ and monotonically decreases with height. In Model C, it has a value of zero at the ground, rises to a peak value and then decreases slowly back to zero at the top of the cloud.

These changes in the Richardson number submodel significantly changed the predicted velocity fields within the first two meters downwind of the source. Fig. 3 is a close-up view of the predicted velocity fields behind the source, using the three K-theory models described earlier. Model A has produced three vortices, Model B has only one, and Model C has no apparent vortices. Unfortunately, no experimental measurements are available for comparisons. However, based on the results shown in Figs. 5 - 7, the vortices shown in Fig. 3(a) are apparently unreal, and the velocity field produced by Model C in Fig. 3(c) is probably a good representation of the real flow field. As previously stated, the Richardson number obtained with Model A was much too large behind the source, due primarily to the inappropriate scaling of the friction velocity in this region. The use of a constant friction velocity (the value of the ambient atmosphere) in the other two models has apparently contributed to the much improved results in Figs 3(b) and 3(c).

Shown in Fig. 4 are the predicted concentration fields. Again, the most difference occurs behind the source region where the turbulence level has been perturbed the most. Sufficiently far from the source, the discrepancies are generally smaller. One can, however, note the difference in the vertical concentration gradients as shown by the spacing between contour levels. For example, in the top half of the cloud, the gradient is steeper (closer contours) in Model C than that in both Models A and B. Additional comments regarding the concentration gradients will be made in the discussion of the concentration profile shown in a later figure.

The predicted ground level concentrations and measured data are compared in Fig. 5. As is seen, Model A has vastly overpredicted the concentration for a downwind distance up to approximately 2 m behind the source. Such a high concentration zone is apparently a consequence of the spurious vortices created by Model A. On the other hand, results from both Models B and C are in much better agreement with the measured data.

In Fig. 6, a comparison is made for the value of λ (which corresponds to a height with 50% concentration of that on the ground) versus downwind distance. Model A, for the most part, underpredicts the value of λ. Although the results from Model B appear to agree reasonably well with those from Model C in ground concentrations (see Fig. 5), Model B is obviously not

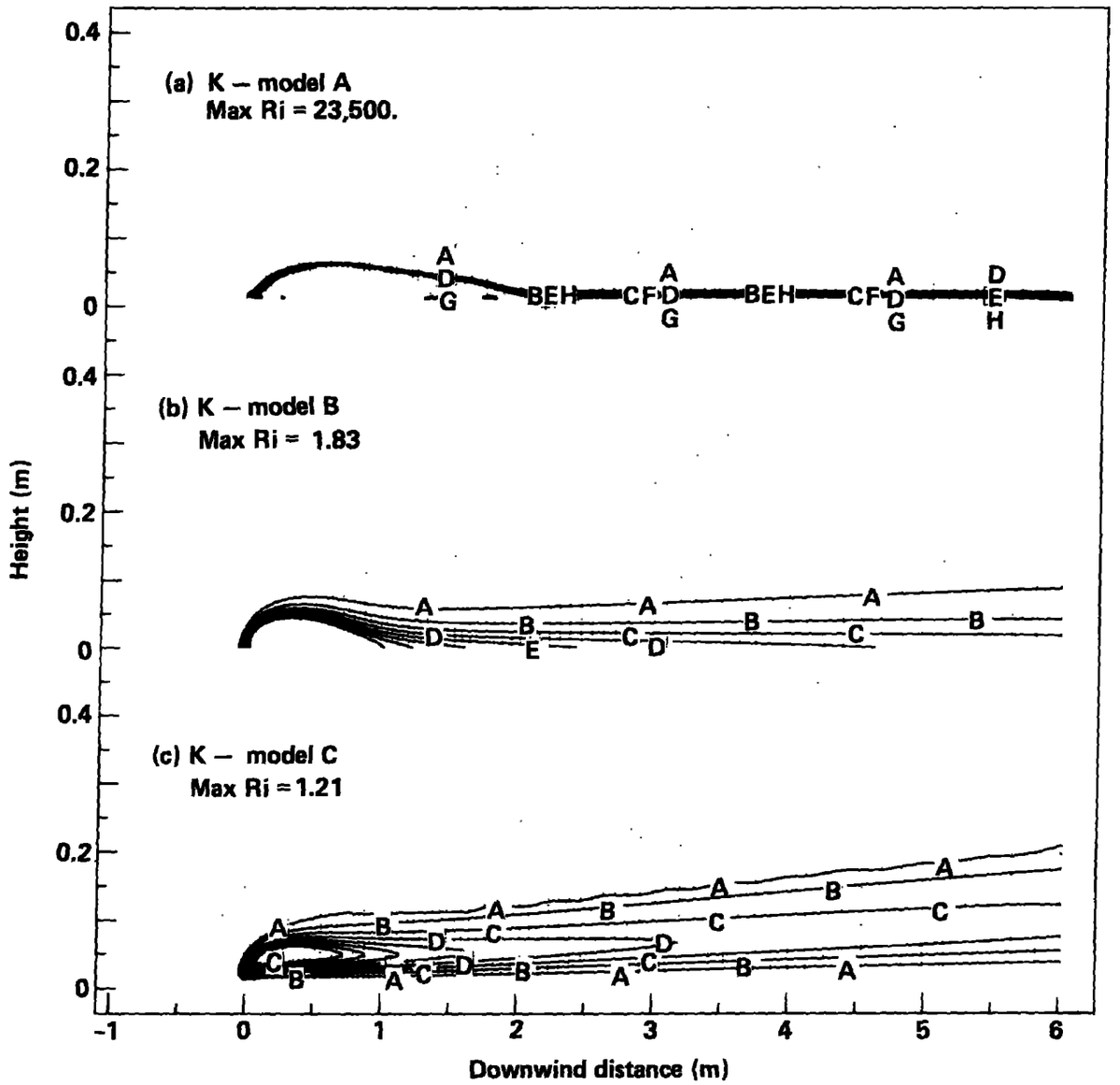

Fig. 2. Predicted Richardson number contours for McQuaid's Experiment No. 3. Contour levels are: A = .1, B = .2, C = .3, D = .4, E = .5, F = .6, G = .7, H = .8.

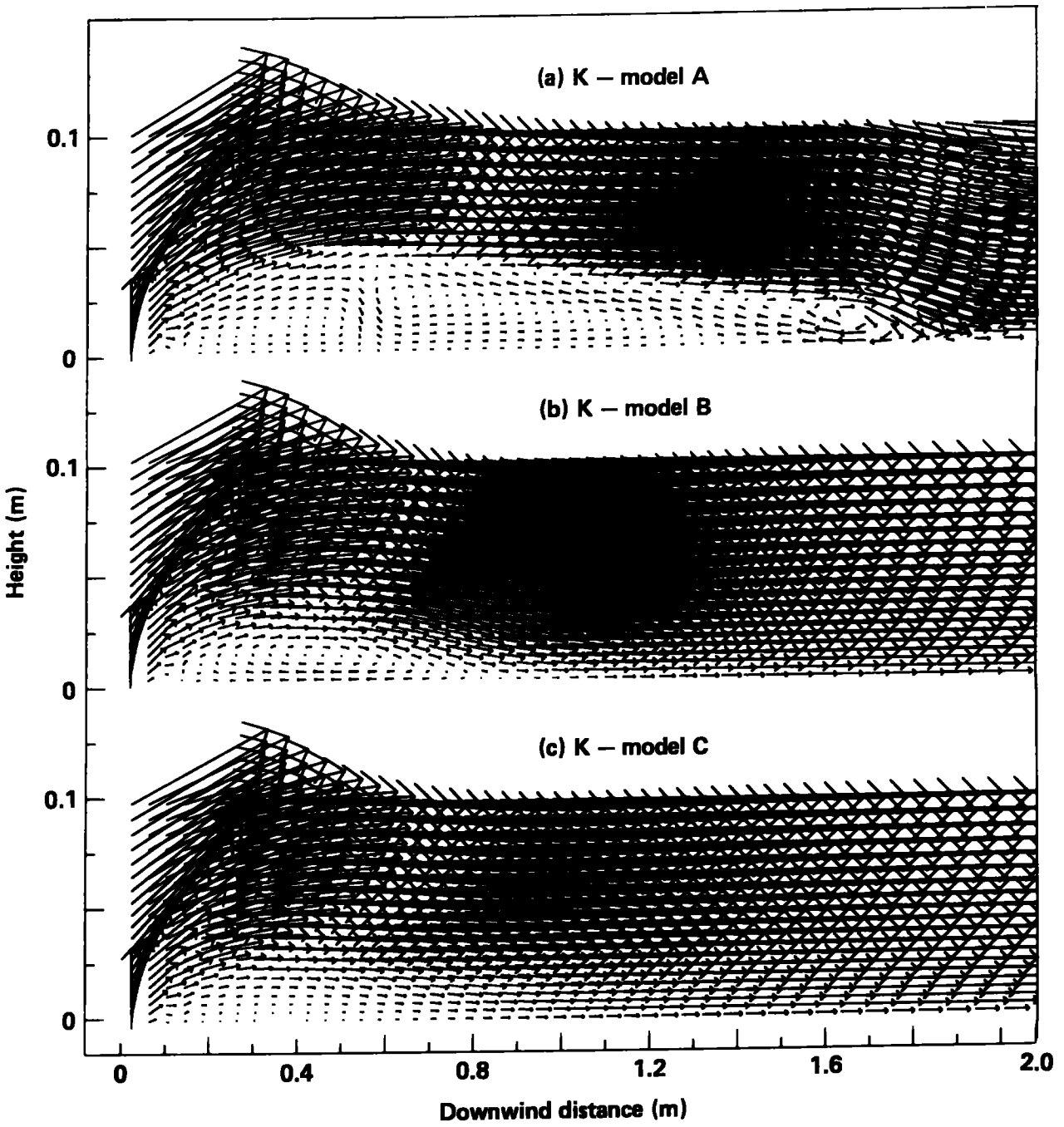

Fig. 3. Predicted velocity vectors behind the source for McQuaid's Experiment No. 3.

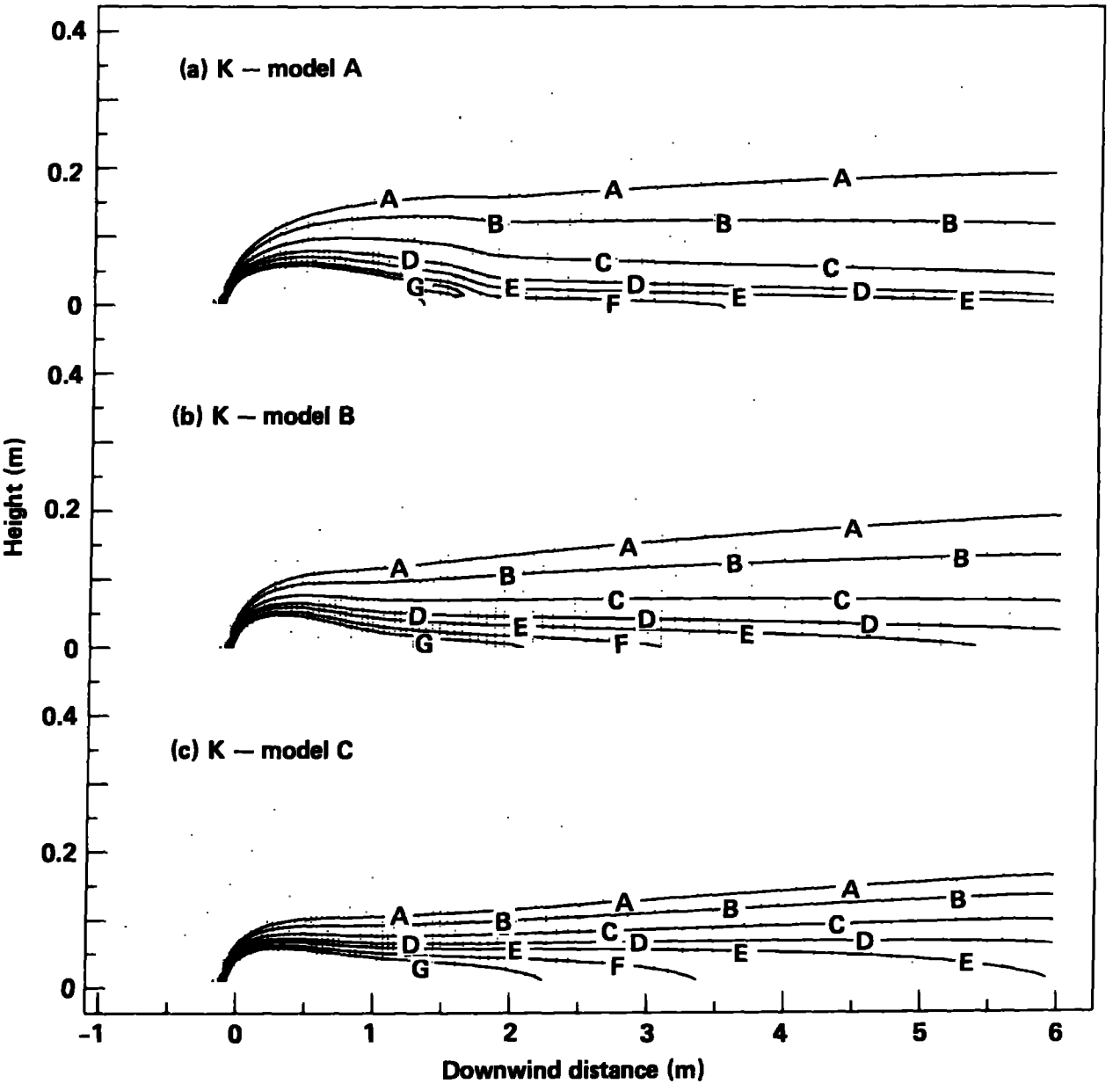

Fig. 4. Predicted CO_2 concentration contours for McQuaid's Experiment No. 3. Contour levels are: A = 0.01, B = 0.02, C = 0.05, D = 0.10, E = 0.15, F = 0.25, G = 0.35.

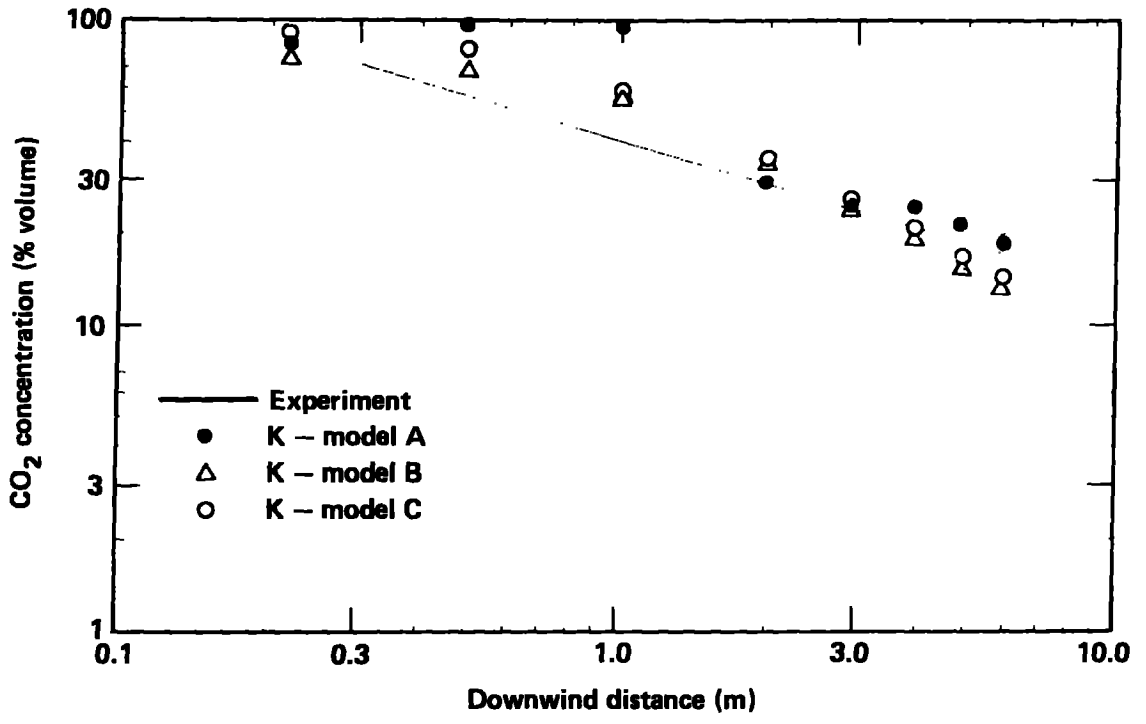

Fig. 5. Comparison of measured and predicted ground level CO_2 concentrations for McQuaid's Experiment No. 3.

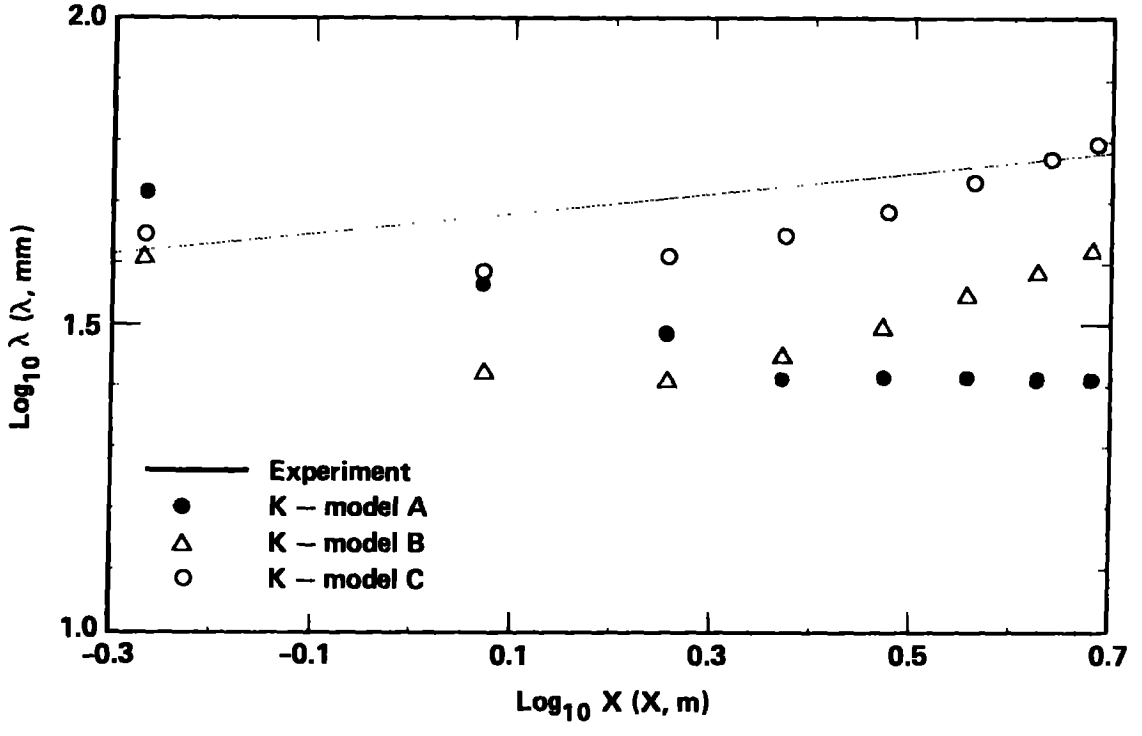

Fig. 6. Comparison of measured and predicted values of λ (the height with 50% ground level concentration) for McQuaid's Experiment No. 3.

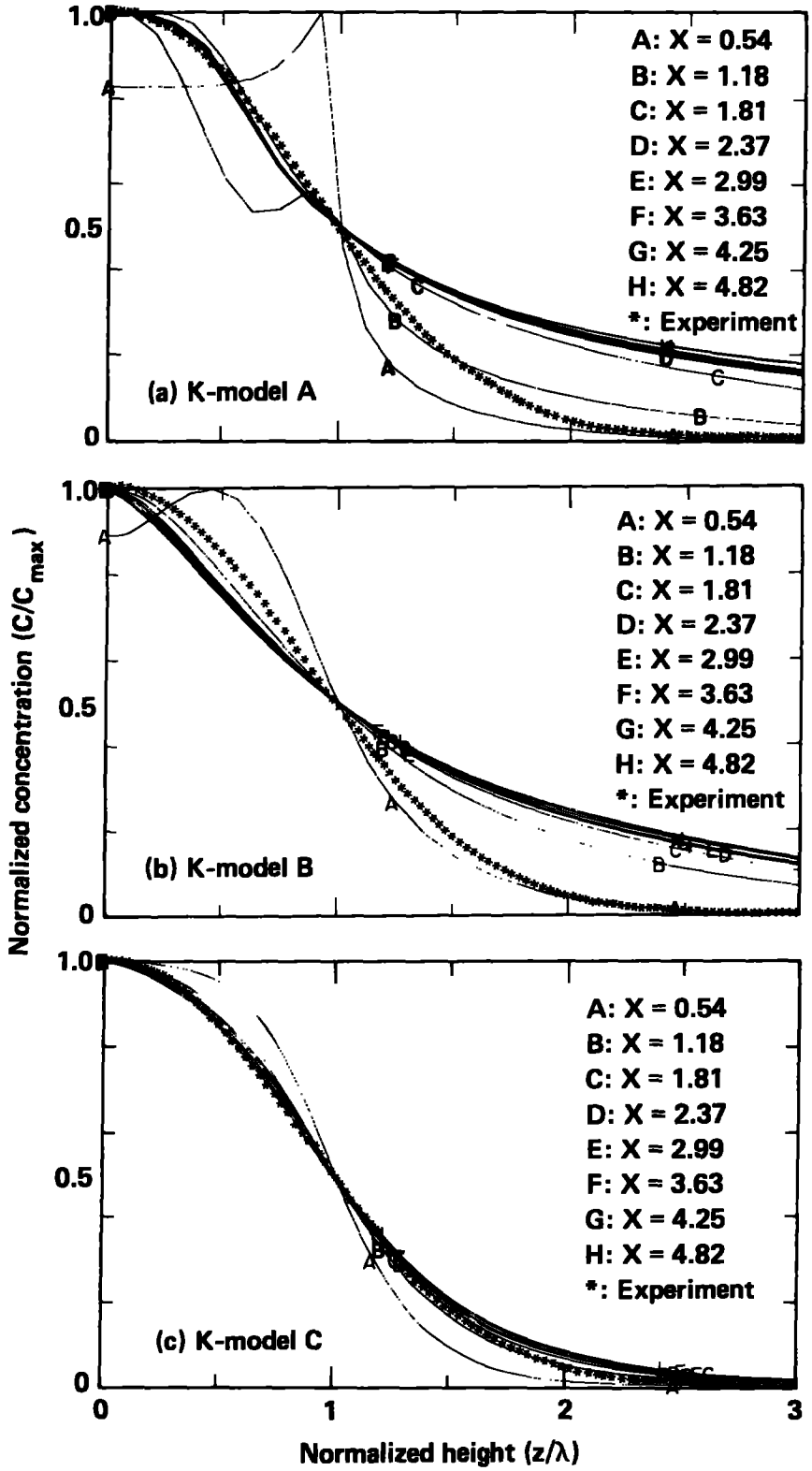

Fig. 7. Comparison of measured and predicted concentration profiles at various downwind locations for McQuaid's Experiment No. 3.

performing as well as Model C in predicting the cloud shape (in terms of the height of λ).

The predicted concentration profiles at different downwind distances from the source are shown in Fig. 7. The profiles for the first two stations ($x < 1.2$ m) from Model A are vastly in error, and those for the remaining stations are significantly flatter than the measured data for heights above λ. A similar cloud shape is predicted by Model B for most of the stations; however, compared to Model A the cloud profiles for the close-in stations are in much better agreement with measurements. In the lower half of the cloud ($\lambda < 1.0$) the gradient is too steep resulting in lower concentrations and in the upper half of the cloud the gradient is too low resulting in higher concentrations than observed in the experiment. Finally, with Model C, the agreement between predictions and measured data is remarkably good except at the first station, where the model appears to be underpredicting the turbulence mixing of the cloud.

Similar results have been obtained for Experiment No. 2 and are shown in Figs. 8 - 13. The Richardson number was, in general, significantly lower in Experiment No. 2 than it was in Experiment No. 3. Comparing the Richardson number from Experiment No. 2 (Fig. 8) with that from Experiment No. 3 (Fig. 2), the maximum value was reduced by a factor of 200 for Model A and a factor of 3 - 4 for Models B and C. Consequently, dense gas effects are somewhat less important in this case and the ambient turbulence level is not altered as much as that in Experiment No. 3.

This is clearly demonstrated in Fig. 9 which shows the velocity vector field in the first two meters behind the source. Over most of this region, the velocity field remains unperturbed even for Model A where only one small vortice exists within the first half meter behind the source. The flow field is less perturbed in the calculations with Models B and C, and the difference between the two results appears to be quite small. There were no vortices produced in the Model B and C simulations.

The difference in the predicted concentration between Models B and C was also quite small, as can be seen in both Figs. 10 and 11. With regard to ground-level concentration, the Model B values were generally less than the

Model A values, and the Model C values were less than those of Model B, although only slightly. Since this trend resulted in increasingly better agreement with the data, this suggests that the physical assumptions used in developing Model C are more in agreement with physical reality than those used in Model B and even more so than those used in Model A. The increasing agreement from model to model is also shown in Fig. 12, which shows a comparison of the measured and predicted values of the cloud height parameter λ versus the logarithm of downwind distance. The Model C results are seen to be in very good agreement with the measured values.

The successively better agreement between measurement and prediction in going from Model A to Model C is also shown in Fig. 13 where the normalized concentration distribution is plotted versus normalized height for a number of downwind distances. The wide excursions from the measured profile that occurred in the simulations of Experiment No. 3 with Model A and B at the first few downwind locations did not occur in Experiment No. 2 due to the decreased importance of dense gas effects in this test. Except for the first few downwind locations in the Model A simulation, the vertical profile at successive downwind locations tends to maintain a constant shape for each model. However, for Model C, that shape is very close to the new Gaussian (exponent = 2.14) profile measured in the experiments, while for Models A and B that shape is closer to an exponential (exponent = 1.00) profile.

In general, both Models B and C provide a significant improvement over Model A. In a comparison between Models B and C, for some criteria Model C is significantly better than Model B, while for others it is only slightly better. For example, the Model C predictions of λ versus downwind distance (Figs. 6 and 12) and the concentration profile as a function of height (Figs. 7 and 13) are significantly better than the Model B predictions. On the other hand, the Model B predictions of maximum concentration versus downwind distance (Figs. 5 and 11) are essentially as good as those from Model C. This suggests that model-data comparisons regarding cloud structure are a more rigorous test of the model than comparisons based on the maximum concentration. These results also suggest that a bulk Richardson number may be sufficient for predictions of maximum concentration, but it is generally not sufficient for the accurate predictions of cloud structure.

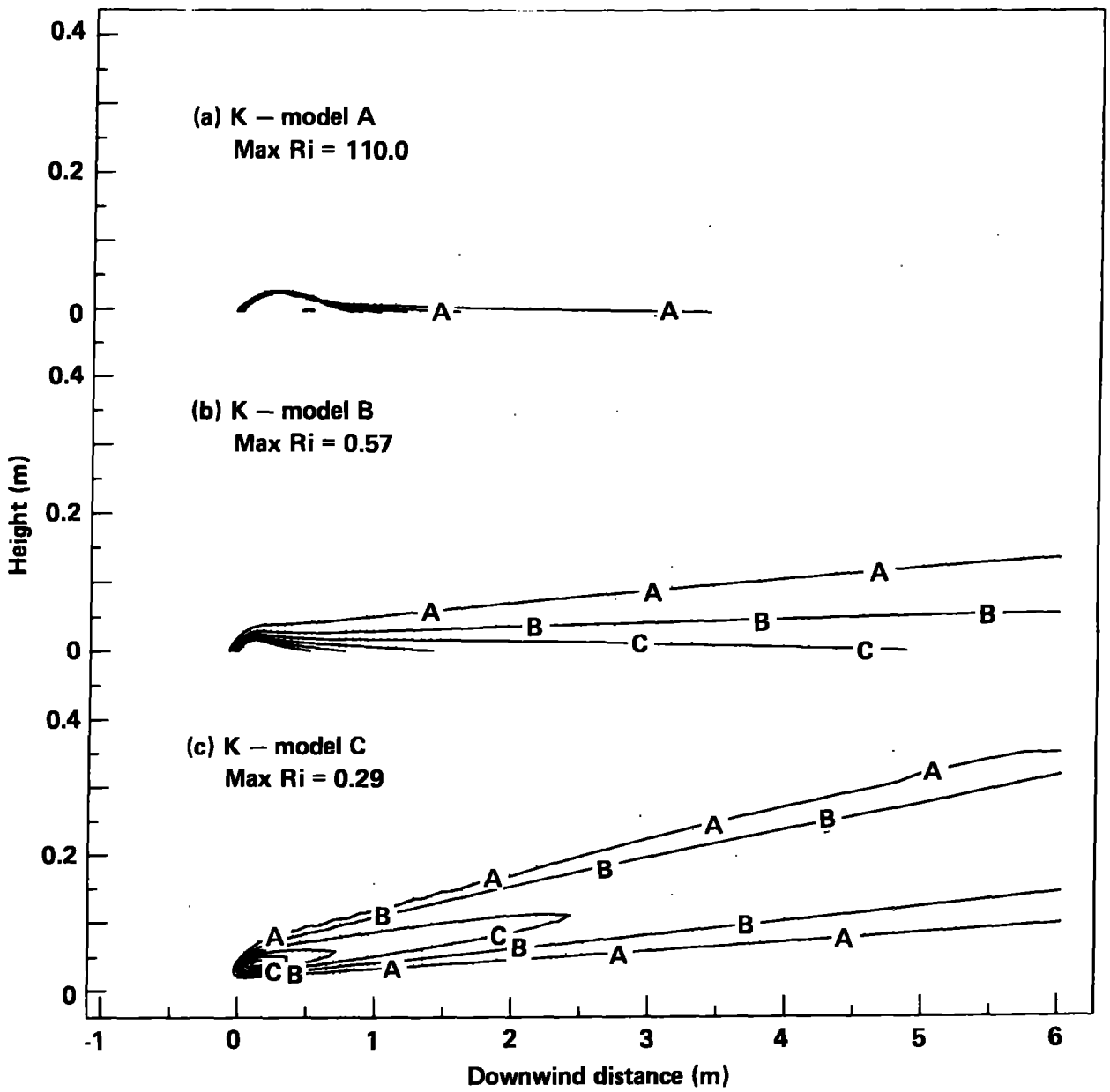

Fig. 8. Predicted Richardson number contours for McQuaid's Experiment No. 2. Contour levels are: A = .04, B = .08, C = .12, D = .16, E = .20, F = .24.

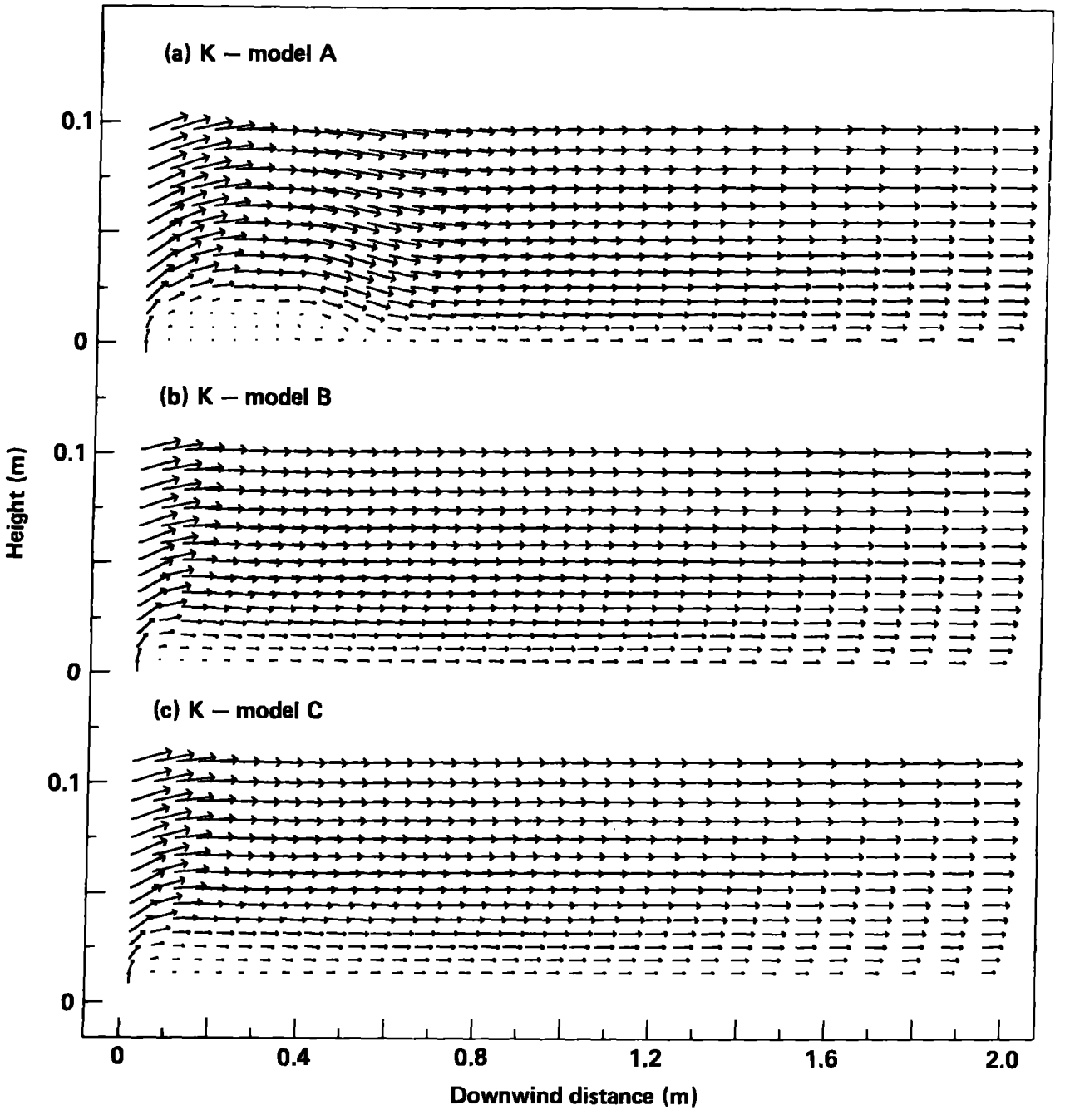

Fig. 9. Predicted velocity vectors behind the source for McQuaid's Experiment No. 2.

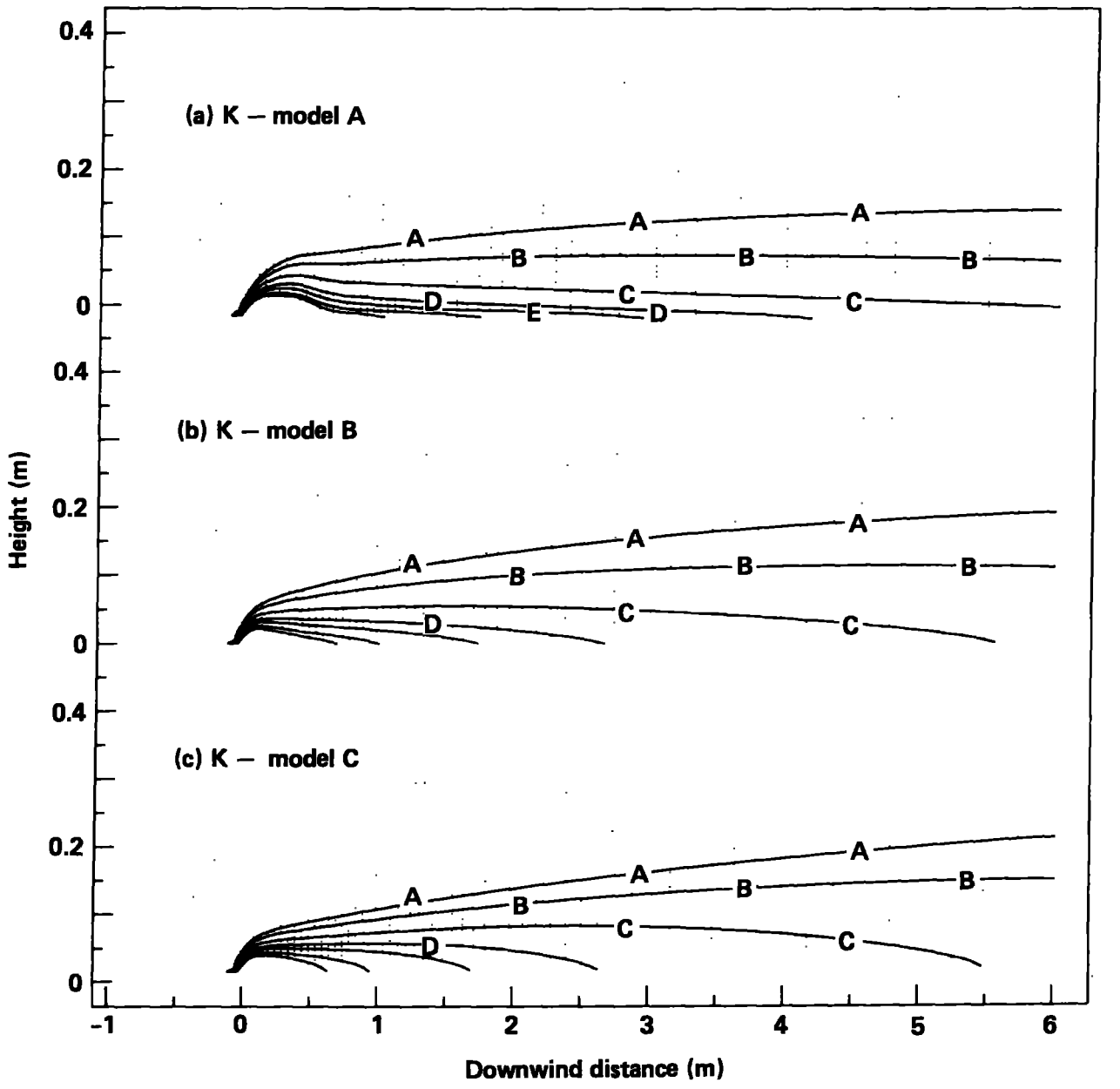

Fig. 10. Predicted CO_2 concentration contours for McQuaid's Experiment No. 2. Contour levels are: A = 0.01, B = 0.02, C = 0.05, D = 0.10, E = 0.15, F = 0.25; G = 0.35.

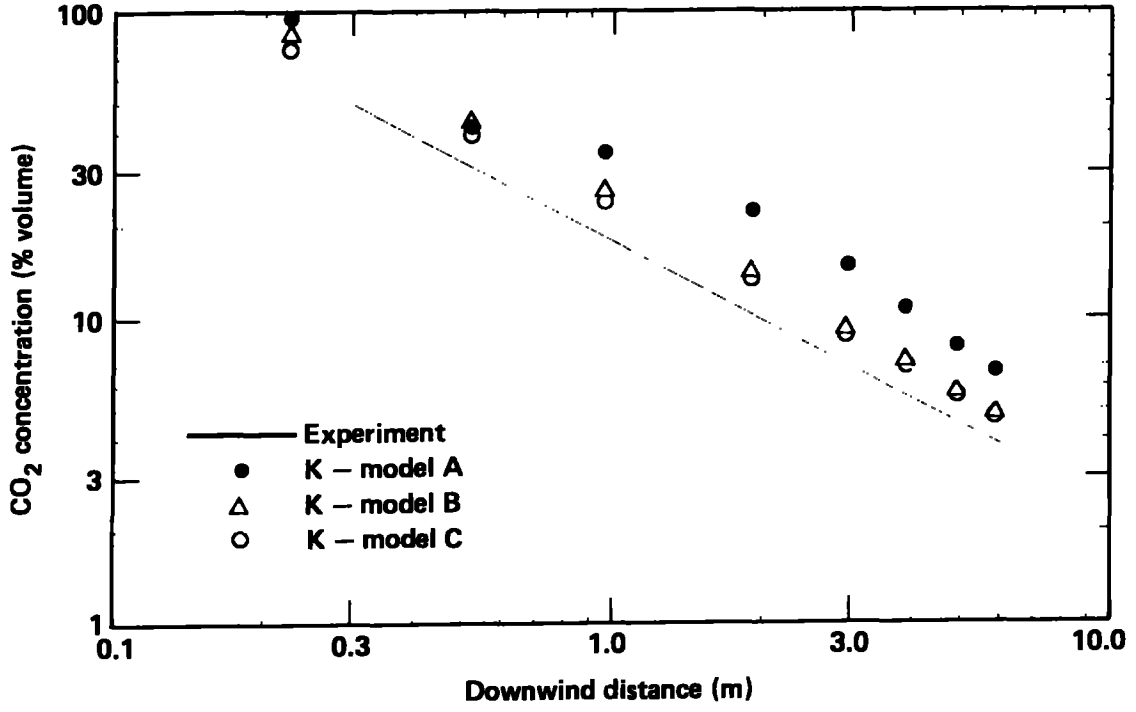

Fig. 11. Comparison of measured and predicted ground level CO_2 concentrations for McQuaid's Experiment No. 2.

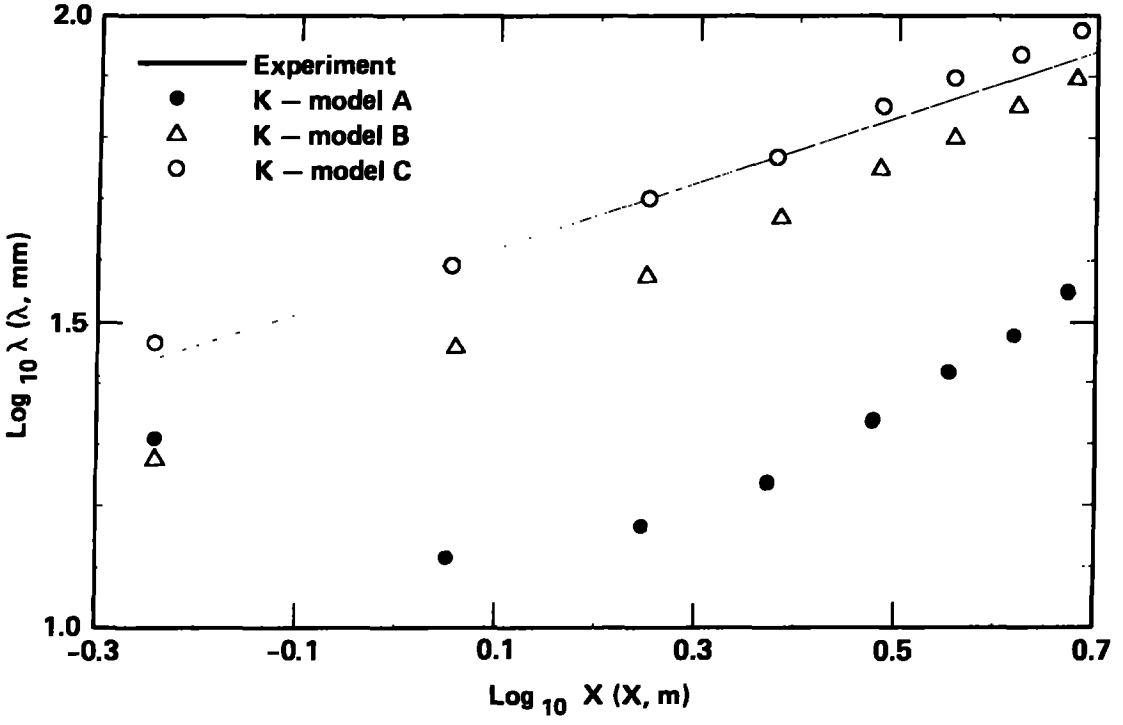

Fig. 12. Comparison of measured and predicted values of λ (the height with 50% ground level concentration) for McQuaid's Experiment No. 2.

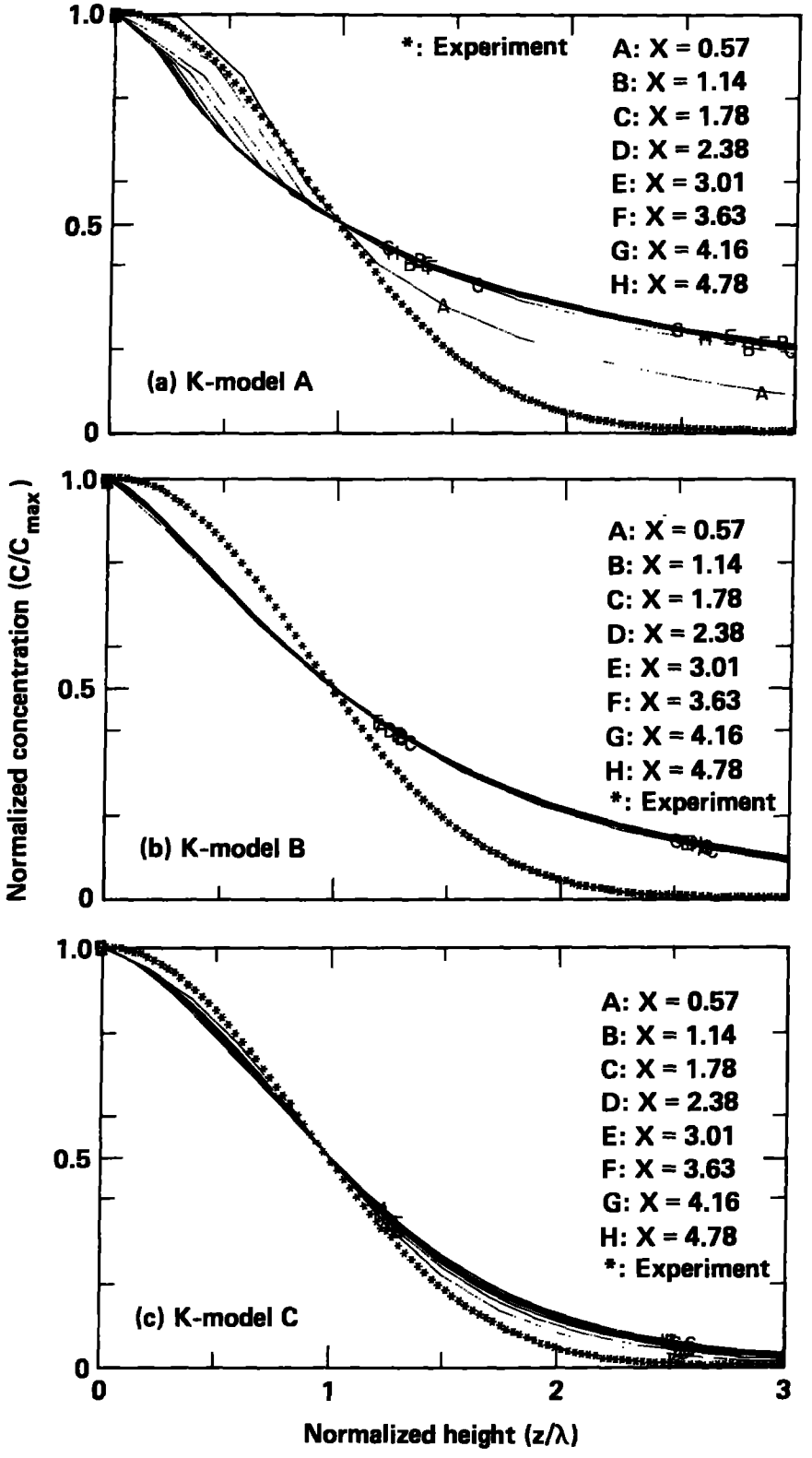

Fig. 13. Comparison of measured and predicted concentration profiles at various downwind locations for McQuaid's Experiment No. 2.

2.4 Vertical Concentration Profile

The vertical concentration profile c(z) generally depends upon the velocity field as well as the turbulent diffusivity. When the terrain is flat, the velocity profile u(z) is essentially a function of the surface roughness and the stability or density stratification of the flow field. The source gas perturbes the ambient flow as the two mix and flow downwind. The excellent agreement obtained in this study suggests that FEM3 is simulating both the diffusivity and velocity field quite accurately. In the wind tunnel tests discussed here, the concentration profile decayed esponentially with a power n = 2.14, suggesting a near Gaussian behavior. While the Gaussian concentration profile has been used extensively to represent the concentration distribution of pollutants dispersing in the atmosphere, this profile is not always observed in heavy gas dispersion experiments.

Indeed, a different profile has been observed in a very similar set of wind tunnel tests. This second series of wind tunnel experiments was conducted by Stretch et al. (1983). Both sets of experiments involved releases of CO_2 from a line source into a low-speed wind tunnel. The geometries were very similar and the source Richardson numbers covered essentially the same range. Yet the concentration profile in the Stretch experiments had a near exponential (n = 1) shape while those in the McQuaid experiments had essentially a Gaussian shape. The reason for this difference is not obvious to us. Presumably, there were differences in the upwind velocity and diffusivity profiles resulting from differences in surface roughness or other turbulence generating mechanisms used in the wind tunnels.

The practical difficulties of measuring the vertical concentration profile in field scale experiments are significantly greater than in the wind tunnel. While the availability of quality data for making this type of analysis is significantly less, a few attemtps have been made using data from dense gas dispersion experiments conducted in the field. Ermak et al. (1982) calculated the vertical concentration profile within the first few hundred meters for one of the Burro LNG spill tests. They found that the concentration profile had an exponential (n = 1) shape for this test and at these downwind distances. This test involved the dispersion of a large

release of liquefied natural gas into a neutral atmosphere with the dispersion occurring over the desert floor. Since LNG vapor is significantly cooler than the ambient atmosphere and the underlying ground, significant heating of the lower layer of the cloud occurred. Consequently, while the LNG cloud as a whole may have formed a stable layer, the lower part of the cloud may have been an unstable region and this may have affected the concentration profile. At further downwind distances, the peak concentrations occur above ground level, suggesting that ground heat had caused the cloud to become positively buoyant.

Another example involving field scale dense gas dispersion experiments is taken from the analysis by Brighton (1985) on the Thorney Island Trials performed by the British Health and Safety Executive. These experiments involved the instantaneous release of a freon air mixture that typically had a density twice that of the ambient atmosphere. In his analysis of the vertical concentration profile, he attempted to fit the data to a modified Gaussian profile given by

$$C(z) = \begin{cases} C_g & , \quad z < h \\ C_g \cdot \exp[-(z - h)^2/2\sigma^2] & , \quad z > h \end{cases}$$

where C_g is the mean ground-level concentration, h is the height of the constant concentration region, and σ is the standard deviation of the Gaussian. In attempting to fit the data to this profile, it was found that most of the time $h < 0$. This suggests that the profile has a shape that corresponds to a value of $n < 2$, although how much less is not possible to say. However, it appears that most of the time the deviations were to a lower value rather than to a larger one.

While the Gaussian profile has been extensively used to represent the oncentration profile for the transport of neutrally buoyant trace emissions, the physical reality of this assumption has been questioned. Holtslag et al. (1985) conducted a theoretical calculation of the concentration profile based upon the advection diffusion equation. In these calculations, he used Monin-Obukhov similarity theory functions taken from Dyer (1974) for the vertical

wind velocity and the vertical eddy diffusivity. Using this model, they calculated the concentration profile as a function of downwind distance and found that the exponent n varied from 0.5 to 2.5 depending upon the surface roughness, atmospheric stability defined by the Monin Obukhov length, and distance downwind. These results indicate that the shape of the concentration profile may not only differ from one test to another, but may also change within the same test.

While the results obtained from the FEM3 Model C calculations were very encouraging, additional comparisons involving tests conducted under different spill, meteorological, and terrain conditions are needed. The few examples cited above demonstrate that the concentration profile may differ considerably, depending upon the meteorological and terrain conditions over which the dispersion occurs. The spill conditions including spill size, relative density, and the mode of spill (continuous or instantaneous) may also affect the concentration profile. Additional assessments are needed to ensure that FEM3 performance continues to be as good as it was in these experiments.

3. CONCLUSIONS

The limited availability of experimental data along with the contrasting need to test models over a wide range of conditions makes the process of atmospheric dispersion model validation a continuing activity involving comparisons with both laboratory-scale and field-scale experiments. The comparisons used in this study involved laboratory-scale tests where detailed measurements of the dense gas cloud structure were made. These detailed comparisons have allowed for the verification and, hopefully, improvement of the turbulence submodel in FEM3. Further validation studies with field-scale experiments are necessary to determine the breadth of these improvements.

The results of this study also suggest that model-data comparisons based on dense gas cloud structure in the vertical direction can be a very useful model validation criterion in addition to comparisons of predicted and observed maximum concentrations. While cloud structure data is generally more difficult to obtain in field scale experiments, it appears to be a rather sensitive test of model performance.

4. ACKNOWLEDGEMENTS

The authors would like to thank L.K. Morris for her assistance in graphics support and conducting some of the computations. This work was performed for the United States Air Force Engineering and Services Center, Tyndall AFB (MIPR N86-16) under the auspices of the U.S. Department of Energy by the Lawrence Livermore National Laboratory under contract No. W-7405-ENG-48.

5. REFERENCES

Brighton, P.W.M. (1985) Area-Averaged Concentrations, Height-Scales and Mass Balances, J. of Haz. Materials, 11, 189-208.

Chan, S.T. (1983) FEM3 -- A Finite Element Model for the Simulation of Heavy Gas Dispersion and Incompressible Flow: User's Manual, UCRL-53397, Lawrence Livermore National Laboratory, Livermore, CA.

Chan, S.T. and D.L. Ermak (1985) Further Assessment of FEM3 -- A Numerical Model for the Dispersion of Heavy Gases over Complex Terrain, UCRL-92497, Lawrence Livermore National Laboratory, Livermore, CA. Presented at the 1985 JANNAF S&EP Subcommittee Meeting, Monterey, CA, Nov. 4-8, 1985.

Chan, S.T., H.C. Rodean, and D.L. Ermak (1984) Numerical Simulations of Atmospheric Releases of Heavy Gases over Variable Terrain, Air Pollution Modeling and Its Application III, Plenum Press, 295-341.

Colenbrander, G.W., A.E. Evans, and J.S. Puttock, (1984) Spill Tests of LNG and Refrigerated Liquid Propane on the Sea, Maplin Sands, 1980: Dispersion Data Digests, Shell Thornton Research Center.

Dyer, A.J. (1974) A Review of Flux-Profile Relationships, Boundary-Layer Meteor., 7, 363-372.

Ermak, D.L. and S.T. Chan (1985) A Study of Heavy Gas Effects on the Atmospheric Dispersion of Dense Gases, UCRL-92494, Lawrence Livermore National Laboratory, Livermore, CA. Presented at the 15th NATO/CCMS International Technical Meeting on Air Pollution Modeling and Its Applications, St. Louis, MO, April 15-19, 1985.

Ermak, D.L., S.T. Chan, D.L. Morgan, and L.K. Morris (1982) A Comparison of Dense Gas Dispersion Model Simulations with Burro Series LNG Spill Test Results, J. of Haz. Materials, 6, 129-160.

Ermak, D.L. and S.T. Chan (1986) Recent Developments on the FEM3 and SLAB Atmospheric Dispersion Models, UCRL-94071, Lawrence Livermore National Laboratory, Livermore, CA. Presented at the IMA Conference on Stably Stratified Flows and Dense Gas Dispersion, Chester, England, Apr. 9-10, 1986.

Goldwire, H.C., Jr., T.G. McRae, G.W. Johnson, D.L. Hipple, R.P. Koopman, J.W. McClure, L.K. Morris, and R.T. Cederwall (1985) Desert Tortoise Series Data Report, 1983 Pressurized Ammonia Spills, UCID-20562, Lawrence Livermore National Laboratory, Livermore, CA.

Goldwire, H.C., Jr., H.C. Rodean, R.T. Cederwall, E.J. Kansa, R.P. Koopman, J.W. McClure, T.G. McRae, L.K. Morris, L.M. Kamppinen, R.D. Kiefer, P.A. Urtiew, and C.D. Lind (1983) Coyote Series Data Report, LLNL/NWC 1981 LNG Spill Tests, Dispersion, Vapor Burn, and Rapid Phase Transitions, UCID-19953, Vols. 1 and 2, Lawrence Livermore National Laboratory, Livermore, CA.

Gresho, P.M., S.T. Chan, C. Upson, and R.Lee (1984) A Modified Finite Element Method for Solving the Time-Dependent, Incompressible Navier-Stokes Equations: Part 1 - Theory; Part 2 - Applications, Int. J. Num. Meth. Fluids, 4, 557-598 and 619-640.

Gudiksen, P.H., M.H. Dickerson, S.T. Chan, L.K. Morris, D.L. Ermak, M. Brown, J. Perry, M. Vonada, and L. Robinson (1986), Emergency Response Planning for Potential Accidental Liquid Chlorine Releases, UCRL-53685, Lawrence Livermore National Laboratory, Livermore, CA

Holtslag, A.A.M., S.E. Gryning, J.S. Irwin, B. Sivertsen (1985) Parameterization of the Atmospheric Boundary Layer for Air Pollution Dispersion Models, presented at the 15th NATO/CCMS International Technical Meeting on Air Pollution Modeling and Its Applications, St. Louis, MO, April 15-19, 1985.

Kansa, E.J., D.L. Ermak, S.T. Chan, and H.C. Rodean, (1983) Atmospheric Dispersion of Ammonia: An Ammonia Fog Model, UCRL-88649, Lawrence Livermore National Laboratory, Livermore, CA

Koopman, R.P., R.T. Cederwall, D.L. Ermak, H.C. Goldwire, Jr., W.J. Hogan, J.W. McClure, T.G. McRae, D.L. Morgan, H.C. Rodean, and J.H. Shinn (1982) Analysis of Burro Series 40-m^3 LNG Spill Experiments, J. Haz. Materials, 6, 43-83.

Leone, J.M., Jr., H.C. Rodean, and S.T. Chan (1985) FEM3 Phase Change Model, UCID-20353, Lawrence Livermore National Laboratory, Livermore, CA.

McQuaid, J. (1976) Some Experiments on the Structure of Stably Stratified Sheer Flows, Technical Paper P21, Safety in Mines Research Establishment, Sheffield, U.K.

McRae, T.G. (1985) Analysis and Model/Data Comparisons of Large-Scale Releases of Nitrogen Tetroxide, UCID-20388, Lawrence Livermore National Laboratory, Livermore, CA.

Morgan, D.L., Jr., L.K. Morris, S.T. Chan, D.L.Ermak, T.G. McRae, R.T. Cederwall, R.P. Koopman, H.C. Goldwire, Jr., J.W. McClure, and W.J. Hogan (1984) Phenomenology and Modeling of Liquefied Natural Gas Vapor Dispersion, UCRL-53581, Lawrence Livermore National Laboratory, Livermore, CA.

Puttock, J.S., G.W. Colenbrander, and D.R. Blackmore (1982) Maplin Sands Experiments 1980: Dispersion Results from Continuous Releases of Refrigerated Liquid Propane, Heavy Gas and Risk Assessment - II, D. Reidel Publ. Co., 147-161.

Stretch, D.D., R.E. Britter, and J.C.S. Hunt (1983) The Dispersion of Slightly Dense Contaminants, IUTAM Symposium, Delft, The Netherlands, 1983, Proceedings; also in Atmospheric Dispersion of Heavy Gases and Small Particles, G. Ooms and H. Tennekes, Eds., Springer-Verlag, New York.